

# Exceptional Points in a Non-Hermitian Topological Pump

Wenchao Hu,<sup>1,2,\*</sup> Hailong Wang,<sup>3,\*</sup> Perry Ping Shum,<sup>1,2</sup> and Y. D. Chong<sup>1,3,†</sup>

<sup>1</sup>Centre for Disruptive Photonic Technologies, Nanyang Technological University, Singapore 637371, Singapore

<sup>2</sup>School of Electrical and Electronic Engineering,

Nanyang Technological University, 50 Nanyang Avenue, 639798, Singapore

<sup>3</sup>Division of Physics and Applied Physics, School of Physical and Mathematical Sciences, Nanyang Technological University, Singapore 637371, Singapore

We investigate the effects of non-Hermiticity on topological pumping, and uncover a connection between a topological edge invariant based on topological pumping and the winding numbers of exceptional points. In Hermitian lattices, it is known that the topologically nontrivial regime of the topological pump only arises in the infinite-system limit. In finite non-Hermitian lattices, however, topologically nontrivial behavior can also appear. We show that this can be understood in terms of the effects of encircling a pair of exceptional points during a pumping cycle. This phenomenon is observed experimentally, in a non-Hermitian microwave network containing variable gain amplifiers.

PACS numbers: 42.60.Da, 42.70.Qs, 73.43.-f

## I. INTRODUCTION

The existence of topologically distinct phases of matter was one of the most profound discoveries of theoretical physics in recent decades.<sup>1</sup> The idea of classifying bandstructures using topological invariants, such as the Chern number,<sup>2</sup> arose originally in the study of the quantum Hall effect,<sup>3</sup> and subsequently led to the discovery of two- and three-dimensional topologically insulating materials. It has also inspired numerous proposals and experiments for realizing topologically non-trivial bands using light,<sup>4</sup> sound,<sup>5,6</sup> and other types of waves.<sup>7</sup> According to the topological bulk-edge correspondence principle,<sup>8</sup> topologically nontrivial bandstructures imply the existence of topologically-protected edge states, whose unique transport properties may have applications in many fields.

Theories of bandstructure topology typically assume that the underlying lattice is Hermitian. Yet in settings such as topological photonics, non-Hermitian effects—in the form of gain and/or loss—are easily introduced, and may be both substantial and unavoidable in practical implementations.<sup>9</sup> Broadly speaking, non-Hermiticity poses two problems for standard theories. Firstly, non-Hermitian bands can exhibit exceptional points (EPs),<sup>10,11</sup> in which case bands cease to be continuously single-valued throughout  $k$ -space, which is conceptually troublesome for band invariants such as Chern numbers. Secondly, standard formulations of the bulk-edge correspondence principle rely on the existence of a real spectral gap in the bulk. For instance, in Hatsugai's well-known derivation of the correspondence between quantum Hall edge states and Chern numbers, it is crucial to assume that a lattice in a strip geometry has a *real* point spectrum which converges, in the large-system limit, to an integer number of real bands.<sup>12</sup>

A number of recent works<sup>13–18</sup> have started to explore how band topological ideas might be extended to non-Hermitian systems. Notably, certain special one- and two-dimensional non-Hermitian lattices have been found to exhibit topological invariants with meaningful bulk-

edge correspondences.<sup>17,18</sup> Some of these novel invariants are based on the integral winding numbers associated with EPs of the complex band spectrum (i.e., branch point orders), which constitute a natural class of discrete features tied to non-Hermiticity. So far, however, it has been unclear whether there is a connection between invariants based on EP winding numbers and the standard topological invariants previously developed for Hermitian systems.

This paper demonstrates, theoretically and experimentally, a relationship between a previously-known Hermitian topological invariant and EP winding numbers. The topological invariant comes from a *topological pump*,<sup>19–23</sup> in the form of the winding numbers of scattering matrix eigenvalues during a parametric pumping cycle.<sup>24</sup> In a Hermitian lattice, the bulk-edge correspondence principle associates a zero (nonzero) winding number with a topologically trivial (nontrivial) bulk bandgap. Strictly speaking, however, topologically nontrivial behavior emerges only in the  $N \rightarrow \infty$  limit, where  $N$  is the sample width (i.e., the limit where opposite edges of the sample are decoupled). We show that when the topological pump is continued into the non-Hermitian case, e.g. by applying both gain and loss, topologically nontrivial behavior can arise under the generalized condition

$$|\gamma| \gtrsim e^{-N}, \quad (1)$$

where  $\gamma$  parameterizes the non-Hermiticity (gain/loss) in each unit cell. In the Hermitian case ( $|\gamma| \rightarrow 0$ ), satisfying (1) requires taking  $N \rightarrow \infty$ . For a non-Hermitian lattice ( $\gamma \neq 0$ ), nonzero windings can occur for finite  $N$ , and we show that these emerge out of the winding numbers of a pair of EPs of the non-unitary scattering matrix.

The above ideas are realized and confirmed in an experiment on a classical electromagnetic network in a topological pumping configuration,<sup>19–21</sup> operating in the microwave frequency range (900 MHz). Previously, we have shown that such a network, constructed from radio frequency (RF) cables, couplers, and phase shifters, can be used to implement a topological pump.<sup>24</sup> The windings

of the scattering matrix eigenvalues, during a pumping cycle, were found to match the underlying bandstructure of the network, which could be topologically trivial or nontrivial. In that experiment, the intrinsic losses were fixed.<sup>24</sup> Here, we incorporate *tunable* amplifiers that can be used to control the level of non-Hermiticity. This allows us to probe for the theoretically-predicted EPs, and study their effects on the topological pump.

## II. EXCEPTIONAL POINTS AND TOPOLOGICAL PUMPING

We begin with a theoretical analysis of a 2D square-lattice network of directed links joined by nodes, shown in Fig. 1(a). Steady-state waves propagating in the links are described by complex scalar amplitudes; at each node, the input and output amplitudes are related by a  $2 \times 2$  coupling matrix. As shown in previous works,<sup>30</sup> if all links have line delay  $\phi$ , wave propagation in an infinite periodic network is described by the Floquet equation

$$U(\mathbf{k})|\psi(\mathbf{k})\rangle = e^{-i\phi}|\psi(\mathbf{k})\rangle. \quad (2)$$

For a Bloch state with real crystal wave-vector  $\mathbf{k}$ ,  $|\psi(\mathbf{k})\rangle$  denotes a vector of wave amplitudes exiting the nodes of one unit cell in the network, and  $U(\mathbf{k})$  describes the “scattering” of the wave by the unit cell. Eq. (2) thus describes a Floquet bandstructure, with  $\phi(\mathbf{k})$  as a quasienergy.

The network is “Hermitian” if there is no gain or loss, so that all propagation and scattering processes are unitary. Then  $U(\mathbf{k})$  is unitary, and the Floquet Hamiltonian  $H_F(\mathbf{k}) = i\log[U(\mathbf{k})]$  is Hermitian. Moreover, the quasienergies  $\phi(\mathbf{k})$  are real, and the bandstructure can be topologically trivial or non-trivial, depending on system parameters like nodal coupling strengths. (The topologically non-trivial phase is an “anomalous Floquet insulator”, with interesting properties that have been studied in previous works.)<sup>25–31</sup>

A topological edge invariant can be formulated for the network by truncating it in the  $y$  direction to form a strip  $N$  cells wide. Dirichlet boundary conditions are imposed on the upper and lower edges, so that no waves enter or leave via these edges. Translational invariance in  $x$  gives a conserved wave-number  $k$ , equivalent to taking one unit cell along  $x$  and imposing twisted boundary conditions. One can then calculate the bandstructure  $\phi(k)$ , and count the net number of edge states on each edge and in each bandgap. This is a topological invariant, independent of the choice of truncation direction for the strip.<sup>12</sup>

Another way to formulate a topological edge invariant is the Laughlin-Brouwer topological pump.<sup>19–21</sup> As shown in Fig. 1(b), instead of imposing Dirichlet boundary conditions on the edges, we attach scattering leads. The wave amplitudes incident on the two edges,  $|\psi_{\text{in}}\rangle$ , can be related to the output amplitudes  $|\psi_{\text{out}}\rangle$  by

$$|\psi_{\text{out}}\rangle = S_{\text{edge}}|\psi_{\text{in}}\rangle. \quad (3)$$

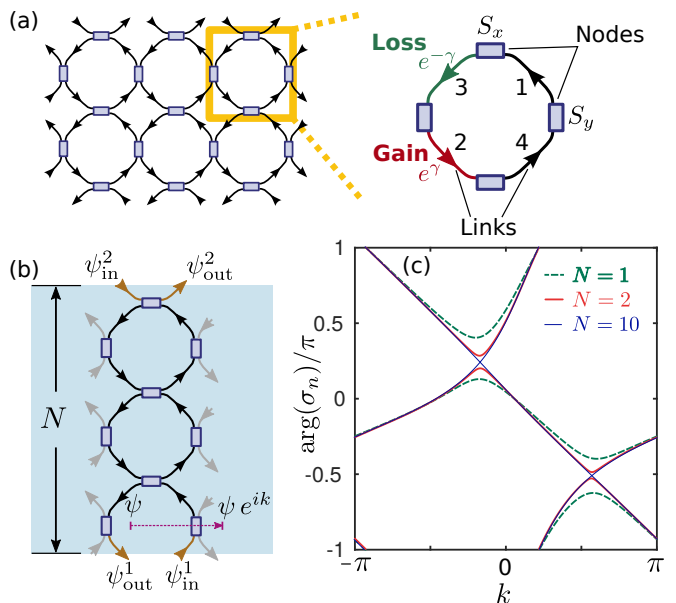


FIG. 1. (a) Schematic of a periodic network of directed links and nodes, with tunable gain and loss in two of the links in each unit cell. (b) Schematic of the setup for the Laughlin-Brouwer topological pump. The network is truncated to  $N$  unit cells in the  $y$  direction, and twisted boundary conditions are applied in the  $x$  direction with tunable twist angle  $k$  (corresponding to an infinite strip with fixed wavenumber). (c) Plot of  $\arg(\sigma_n)$  versus  $k$ , where  $\{\sigma_n\}$  are the eigenvalues of the edge scattering matrix. The model parameters are  $\gamma = 0$  (Hermitian network),  $\theta_x = \theta_y = 3\pi/8$ ,  $\Phi_x^3 = \Phi_y^3 = -7\pi/10$ , and  $\phi = 2\pi/5$ ; these parameters are defined in Appendix A.

The derivation of  $S_{\text{edge}}$  is described in Appendix A. If the network is Hermitian,  $S_{\text{edge}}$  is unitary and its eigenvalues  $\{\sigma_n\}$  lie on the complex unit circle. To perform topological pumping, we set  $\phi$  in a bandgap and advance  $k$  by  $2\pi$ , and then count the resulting winding number of the  $\sigma_n$ 's along the unit circle.<sup>20,21</sup>

Fig. 1(c) plots  $\arg(\sigma_n)$  versus  $k$  for various strip widths  $N$  for the Hermitian network. All the other system parameters are chosen so that the underlying bulk bandstructure is topologically nontrivial and  $\phi \in \mathbb{R}$  lies in a bandgap. For small  $N$ , the individual eigenvalues have *zero* winding around the origin during one cycle of the pumping parameter  $k$ . For larger  $N$ , the points of nearest separation between the eigenvalues appear to shrink. To study this in greater detail, Fig. 2(a) plots  $\Delta \equiv \min|\arg[\sigma_1(k)] - \arg[\sigma_2(k)]|$ , where the minimum is calculated over  $k \in [-\pi, \pi]$ , for various finite  $N$ . This quantifies the minimum separation between the two eigenvalue trajectories, and must vanish if the eigenvalues cross somewhere in  $k \in [-\pi, \pi]$  (which is required for nonzero windings). These numerical results show that  $\Delta \sim \exp(-N)$ , reaching zero only for  $N \rightarrow \infty$ . Physically, this reflects the fact that topological protection is spoiled by the coupling of edge states on opposite edges of the sample; since edge state wavefunctions decay exponentially into the bulk, the coupling strength decreases

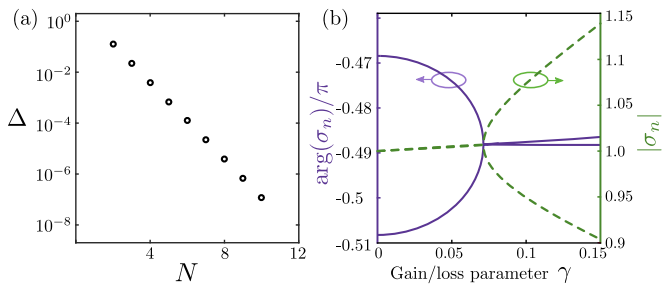


FIG. 2. (a) The gaps between arguments of scattering matrix eigenvalues,  $\Delta \equiv \min(|\arg(\sigma_1) - \arg(\sigma_2)|)$ , in the Hermitian limit  $\gamma = 0$ . Circles represent gaps for different  $N$ . (b) Scattering matrix eigenvalues of the non-Hermitian 2D network, at  $k_{ep} \simeq 0.572\pi$  and  $N = 2$ . The left and right axes show the arguments and amplitudes of the eigenvalues, respectively. The other model parameters are same as in Fig. 1 (c):  $\theta_x = \theta_y = 3\pi/8$ ,  $\Phi_x^3 = \Phi_y^3 = -7\pi/10$ , and  $\phi = 2\pi/5$ .

exponentially with  $N$ .

What is the effect of the above topological pumping process on a non-Hermitian network? To study this problem, we focus on non-Hermitian networks with a specific distribution of gain and loss, shown in Fig. 1(a): in each unit cell, link 2 has gain factor  $\exp(\gamma)$ , link 3 has loss factor  $\exp(-\gamma)$ , and the other links remain unitary. Thus,  $\gamma$  simultaneously tunes gain and loss in links 2 and 3. This arrangement of gain and loss is chosen so that exceptional points (EPs) of the system are easily accessible, and affect the behavior of the topological pump. (Note that it is not  $\mathcal{PT}$  (parity-time) symmetric;<sup>32–36</sup> in Appendix B, we show that in an alternative  $\mathcal{PT}$  symmetric version of the network, the gain/loss distribution does not affect the topological pump.)

We can fix  $\phi$  and  $\gamma$ , and carry out the “pumping” procedure as before: the parameter  $k$  is advanced by  $2\pi$ , and we examine how the trajectories of  $\{\sigma_n\}$ —the eigenvalues of the non-unitary  $S_{\text{edge}}$  matrices—wind in the complex plane. Note that the variation of  $k$  is a parametric evolution, not a time evolution, so the breakdown of adiabaticity in non-Hermitian systems<sup>37</sup> is not an issue. We now observe an interesting feature of the non-Hermitian pump: nonzero windings can occur for *finite*  $N$ , due to the existence of exceptional points (EPs) of  $S_{\text{edge}}$ .

An EP is a point in a 2D parameter space where a matrix becomes defective and its eigenvectors become linearly dependent.<sup>10,11</sup> Due to the spectral theorem, EPs only appear in non-Hermitian systems. In Fig. 2(b), we plot  $\arg(\sigma_n)$  and  $|\sigma_n|$  against the gain/loss parameter  $\gamma$ , for  $N = 2$  and  $k = 0.572\pi$ . The two eigenvalues exhibit bifurcative behavior characteristic of an EP, coalescing at  $\gamma = 0.071$ . In this case,  $S_{\text{edge}}$  possesses a pair of EPs in the 2D parameter space formed by  $k$  and  $\gamma$ ; one EP is located at  $(k = 0.572\pi, \gamma = 0.071)$ , as seen in Fig. 2(b), while the other EP is located at  $(k = -0.1731\pi, \gamma = 0.1132)$ .

Fig. 3 illustrates how the EPs give rise to the topologically nontrivial regime of the topological pump. Fig. 3(a)

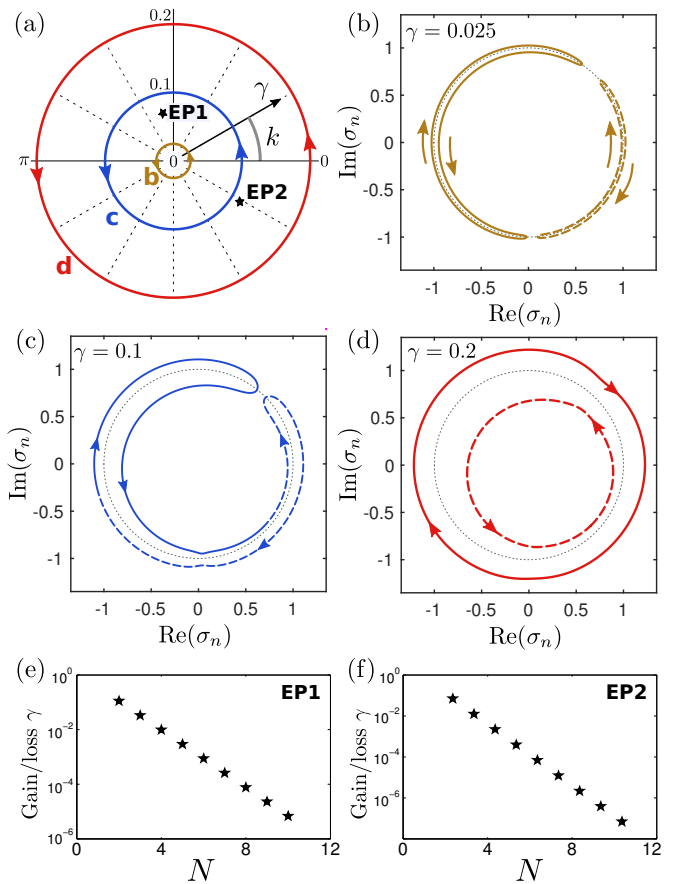


FIG. 3. Relationship between topological pumping and exceptional points, calculated for a network model of width  $N = 2$ . The underlying bandstructure is topologically nontrivial, with  $\phi$  in a bandgap ( $\theta_x = \theta_y = 3\pi/8$ ,  $\Phi_x^3 = \Phi_y^3 = -0.7\pi$ , and  $\phi = 2\pi/5$ ). (a) Parametric loops in the 2D parameter space formed by the gain/loss parameter  $\gamma$  (radial coordinate) and pumping parameter  $k$  (azimuthal coordinate). Exceptional points (EPs) of  $S_{\text{edge}}$  are indicated by stars. (b, c, d) Complex plane trajectories of  $\{\sigma_n\}$ , the eigenvalues of  $S_{\text{edge}}$ , corresponding to the parametric loops shown in (a). The two distinct eigenvalue trajectories are plotted as solid and dashed curves, and the unit circle is plotted as dots for comparison. The trajectories in (b) have zero windings around the origin, like the Hermitian finite- $N$  limit; the trajectories in (c) join each other under one cycle, because the parametric loop encloses one exceptional point; the trajectories in (d) have nonzero windings, similar to the Hermitian large- $N$  limit. (e)–(f) Plots of the gain/loss parameter  $\gamma$  at the two EPs [as labelled in (a)], for different  $N$ .

shows the 2D parameter space, with the gain/loss parameter  $\gamma$  serving as the radial coordinate and the cyclic pumping parameter  $k$  serving as the azimuthal coordinate. The two EPs of  $S_{\text{edge}}$  are labeled EP1 and EP2 (these EP positions depend on  $N$ , which is set here to  $N = 2$ ). In Fig. 3(b)–(d), we plot the trajectories of  $\{\sigma_n\}$  in the complex plane, as the system proceeds along the different parametric loops indicated in Fig. 3(a). For a parametric loop at small  $\gamma$ , not enclosing any EP, the

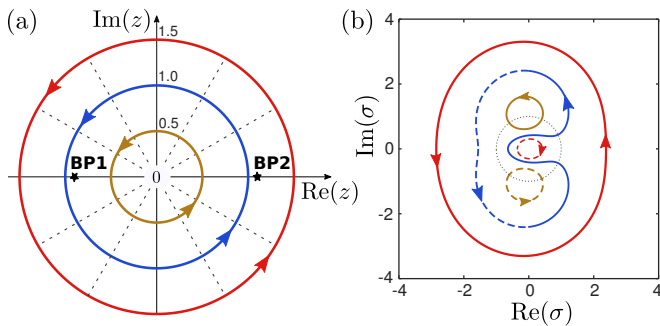


FIG. 4. Behavior of the multi-valued function  $\sigma(z)$  given by Eq. (4), illustrating how branch points can produce winding and non-winding trajectories. Here, we take  $\alpha = 0.1$ . (a) Plot of the parameter space formed by the complex variable  $z$ , with the branch points of  $\sigma(z)$  indicated by stars, along with three parametric loops corresponding to (i)  $|z| = 0.5$ , (ii)  $|z| = 1$ , and (iii)  $|z| = 1.5$ . (b) The corresponding complex plane trajectories of the two branches of  $\sigma(z)$ .

eigenvalue trajectories do not wind around the origin, as shown in Fig. 3(b). This behavior extends down to the previously-discussed Hermitian limit ( $\gamma = 0$ ). For a parametric loop at large  $\gamma$ , enclosing both EPs, the eigenvalue trajectories have nonzero windings, as shown in Fig. 3(d), and is similar to the large- $N$  limit of the Hermitian topological pump. Between these two regimes, there are two points in the parameter space where the eigenvalue trajectories cross, which are EPs of  $S_{\text{edge}}$ . Fig. 3(c) shows the intermediate regime where only one EP is enclosed by the parametric loop. In this case, one pumping cycle induces a continuous exchange of the two eigenvalues, along with their eigenvectors.<sup>11</sup>

We can use a simple model to illustrate how such a mathematical relationship between EPs and eigenvalue windings might arise. Consider the multi-valued function

$$\sigma(z) = z - \alpha + \sqrt{(z - \alpha + 1)(z - \alpha - 1)}. \quad (4)$$

The two branches of  $\sigma(z)$ , arising from the square root, could represent solutions to a secular equation for the eigenvalues of a  $2 \times 2$  matrix, parameterized analytically by a variable  $z$ ; the branch points,  $z = \alpha \pm 1$ , are EPs of that matrix. Fig. 4(a) shows three different loops in the parameter space, centered at  $z = 0$  and enclosing zero, one, and two branch points, similar to Fig. 3(a). In Fig. 4(b), we plot the trajectories of  $\sigma(z)$  corresponding to those parametric loops, and observe winding behaviors very similar to Fig. 3 (b)–(d). In particular, for  $|z| \rightarrow 0$ , branches of Eq. (4) reduce to  $\sigma_{\pm}(z) \approx -\alpha \pm \sqrt{\alpha^2 - 1}$ , exhibiting zero winding during one cycle of  $\arg(z)$ ; whereas for  $|z| \rightarrow \infty$ , the branches reduce to  $\sigma_{\pm}(z) = (2z)^{\pm 1}$ , which wind in opposite directions around the origin.

These findings imply that the topologically nontrivial regime of the Hermitian topological pump<sup>19–21</sup> emerges from the general behavior of the non-Hermitian topological pump, via an appropriate order of limits. For given finite  $N$ , nonzero windings require sufficiently large  $\gamma$ , as

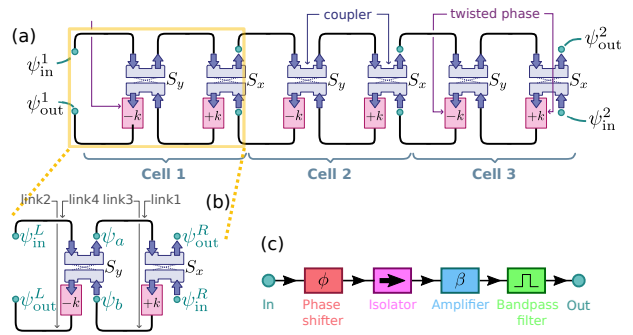


FIG. 5. (a) Experimental setup. Each of the identical units, labeled “Cell 1”, “Cell 2” and “Cell 3,” corresponds to one cell in the topological pump geometry. The twisted boundary condition is applied by tuning phase shifter (pink boxes) in lower links. The couplers (blue rods) are depicted in the strong-coupling configuration. The weak-coupling configuration is achieved by swapping each coupler’s outputs. The overall input and output amplitudes are  $\psi_{\text{in}}^{1,2}$  and  $\psi_{\text{out}}^{1,2}$ . Their scattering parameters are measured with a network analyzer. (b) Each cell is composed of four links ( $j = 1, 2, 3, 4$ ) and two couplers ( $S_x, S_y$ ). (c) Every link in our system are exactly the same and contain one phase shifter, one isolator, one digital controlled variable gain amplifier, one bandpass filter and five low-loss handflex interconnect coaxial RF cables.

expressed in Eq. (1). Fig. 3(e)–(f) shows the values of  $\gamma$  at the EPs for different  $N$ . With increasing  $N$ , the required level of non-Hermiticity decreases exponentially, reaching zero for  $N \rightarrow \infty$ .

### III. EXPERIMENT

In order to realize the non-Hermitian topological pump, we implemented the model described in Section II using a classical electromagnetic network operating at microwave (900 MHz) frequencies. The basic setup is shown in Fig. 5, and is conceptually similar to the experiment previously reported in Ref. 24. The network is designed according to the topological pumping configuration shown in Fig. 1(b). It corresponds to a “column” of the periodic network of width  $N$ , composed of identical unit cells each containing four links and two nodes.

Each directional link consists of five low-loss handflex coaxial RF cables (086-10SM+/086-15SM+, Mini-Circuits), a bandpass filter (CBC-893+, Mini-Circuits), an isolator (S0091IAD, Nova Microwave), a phase shifter (SPHSA-152+, Mini-Circuits), and a digitally-controlled variable-gain amplifier (DVGAI-242+, Mini-Circuits). The link’s transmission coefficient,  $t = \beta \exp(i\varphi)$ , can be independently tuned in both phase and amplitude. The phase  $\varphi \in [0, 2\pi)$  is controlled by the phase shifter with  $\pm 1^\circ$  precision, and is used to set the network model quasienergy  $\phi$  and the pumping parameter  $k$ . The gain/loss factor  $\beta$  is tunable in the range  $[-8 \text{ dB}, 24 \text{ dB}]$  with  $\pm 0.25 \text{ dB}$  precision. The  $-8 \text{ dB}$  lower bound corresponds to turning off the amplifier, and comes from

the intrinsic losses of the components (which are substantially lower than in Ref. 24, due in part to the lower operating frequency of 900 MHz rather than 5 GHz.)

Each node consists of an RF coupler (BDCN-7-25+, Mini-Circuits) with  $\approx 1:7$  coupling ratio. At 900 MHz, its measured  $S$  parameters are

$$S_{\text{coupler}} = \begin{bmatrix} 0.914e^{-i0.622\pi} & 0.348e^{-i0.127\pi} \\ 0.348e^{-i0.127\pi} & 0.914e^{-i0.622\pi} \end{bmatrix}. \quad (5)$$

By swapping the order of the output ports, we can realize both topologically trivial and nontrivial phases of the network model's underlying bandstructure.<sup>24</sup> In terms of the coupling parameter  $\theta$  defined in Appendix A, this means we can set  $\theta \approx 0.12\pi$  (weak-coupling/trivial) or  $\theta \approx 0.38\pi$  (strong-coupling/nontrivial), where  $\theta = 0.5\pi$  is the topological transition point.

To measure the edge scattering matrix,  $S_{\text{edge}}$ , we attach the inputs and outputs at the ends of the ‘‘column’’ to a vector network analyzer (Anritsu 37396C). Fig. 6 shows the results when  $\beta \approx 1$  (i.e., with the amplifiers are tuned so that there is no net gain or loss in each link). In this case,  $S_{\text{edge}}$  is approximately unitary, and as expected the eigenvalues lie very close to the complex unit circle. Under one cycle of  $k$ , we observe no winding in the weak-coupling case. In the strong-coupling case, nonzero windings appear only when the system size is sufficiently large, as shown in Fig. 6(d). This is consistent with the results reported in Ref. 24, and with the theoretical discussion of Section II.

Next, we implement the explicitly non-Hermitian topological pumping configuration discussed in Section II. To do this, we selectively apply amplification to some of the links, according to the gain/loss distribution shown in Fig. 1(a). The results, for  $N = 2$ , are shown in Fig. 7. The parameter space is depicted in Fig. 7(a); our calculations, based on the measured  $S$ -parameters of the individual network components, indicate that there are two EPs very close to  $\beta = 0.4\text{dB}$ . We take three different parametric loops, with results shown in Fig. 7(b)–(d). In Fig. 7(c), the parametric loop passes very close to both EPs, and we observe the two eigenvalue trajectories nearly meeting at two bifurcation points, similar to Fig. 2(b). In Fig. 7(d), when both EPs are enclosed by the parametric loop, the eigenvalue trajectories acquire nonzero windings.

#### IV. SUMMARY

We have performed a theoretical and experimental study of a non-Hermitian topological pump. We have based our study on a network model, which has previously been shown to be a convenient and experimentally feasible way to realize a topological pump using classical microwaves<sup>24</sup>. When gain and loss is added to the network, we find that topologically nontrivial behavior (nonzero windings) requires the pumping process to encircle two exceptional points in the parameter space of

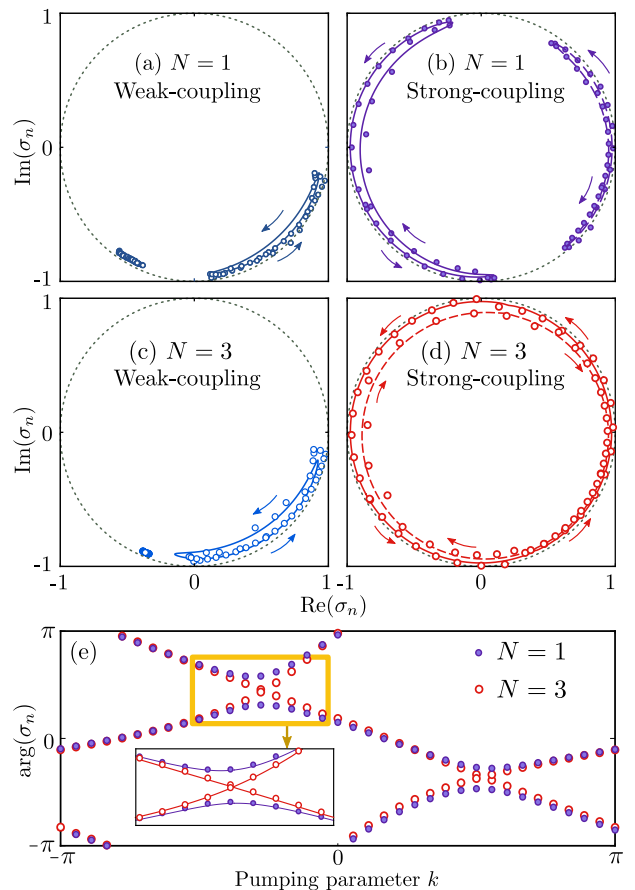


FIG. 6. (a)–(d) Experimentally measured scattering matrix eigenvalues over one pumping cycle, with approximately zero gain/loss. Results are shown for (a,b)  $N = 1$  and (c,d)  $N = 3$ . The weak-coupling regime corresponds to a topologically trivial phase of the underlying network bandstructure, while the strong-coupling regime corresponds to a topologically nontrivial phase. Directly measured data is plotted with dots, and calculations using measured network-component  $S$ -parameters are shown as solid and dashed curves. The unit circle is indicated by dotted curves. (e) Arguments of the measured scattering matrix eigenvalues,  $\arg(\sigma_n)$ , versus pumping parameter  $k$ . The network is in a topologically nontrivial phase. Inset: behavior near a crossing point; solid curves show theoretical results calculated using the network components’ measured  $S$ -parameters, which predict an avoided crossing for  $N = 1$  and a crossing for  $N = 3$ .

the non-Hermitian system. This criterion is a generalization of the  $N \rightarrow \infty$  limit which is necessary for topological protection to emerge in Hermitian topological pumps.<sup>19–21</sup> These theoretical ideas were demonstrated experimentally, using a microwave network containing variable-gain amplifiers. In future work, we seek to generalize this finding to a wider class of non-Hermitian lattices, not necessarily described by network models.

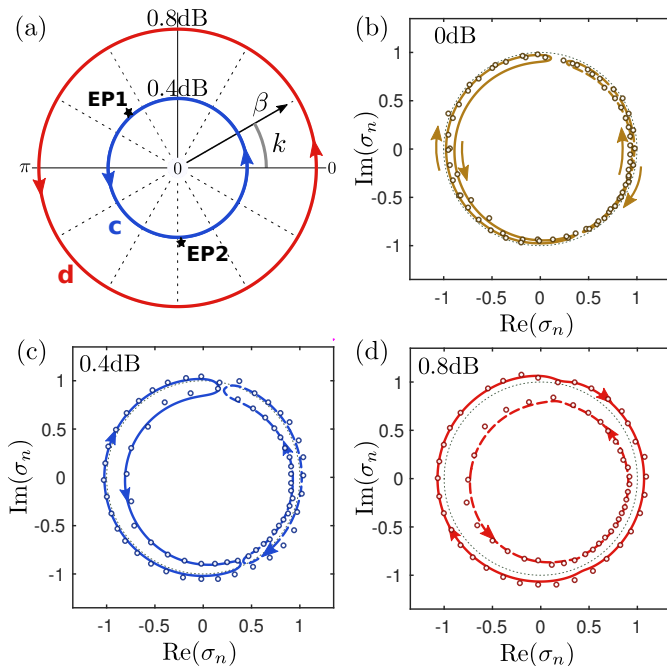


FIG. 7. (a) Parametric loops in the 2D parameter space formed by the logarithmic gain/loss factor  $\beta$  (radial coordinate) and pumping parameter  $k$  (azimuthal coordinate). The gain/loss distribution is as depicted in Fig. 5(a). Exceptional point positions (stars) are calculated from the measured S-parameters of the network components. The system size is  $N = 2$ . (b)–(d) Eigenvalues of  $S_{\text{edge}}$  in the complex plane. Directly measured data is plotted with dots, and calculations using measured network-component S-parameters are shown as solid and dashed curves. The unit circle is indicated by dotted curves.

## V. ACKNOWLEDGEMENTS

We thank Longwen Zhou, Chunli Huang and Daniel Leykam for helpful comments. This research was supported by the Singapore National Research Foundation under grant No. NRFF2012-02, by the Singapore MOE Academic Research Fund Tier 2 Grant No. MOE2015-T2-2-008, and by the Singapore MOE Academic Research Fund Tier 3 grant MOE2011-T3-1-005.

### Appendix A: Scattering matrix of the 2D network

This appendix describes the derivation of the scattering matrix for the network model discussed in Section II. The network is truncated in the  $y$  direction, to form a strip  $N$  cells wide. The periodicity in  $x$  yields a wave-number  $k$ . We can equivalently regard this as a supercell of  $N$  unit cells, with twisted boundary conditions along the  $x$  boundaries with twist angle  $k$ . The supercell can be further divided into  $N$  identical subunits, each composed of four links ( $j = 1, 2, 3, 4$ ) and two couplers ( $S_x, S_y$ ), as shown in Fig. 5(b).

At any given node in the supercell, the incoming and outgoing wave amplitudes are related by a  $2 \times 2$  unitary coupling relation

$$\begin{pmatrix} \psi_{\text{out}}^R \\ e^{-ik-\gamma_3-i\phi}\psi_b \end{pmatrix} = S_x \begin{pmatrix} e^{\gamma_1+i\phi}\psi_a \\ \psi_{\text{in}}^R \end{pmatrix}. \quad (\text{A1})$$

The coupling matrices at the nodes have the simple form

$$S_x = \begin{pmatrix} \sin \theta_x & i \cos \theta_x \\ i \cos \theta_x & \sin \theta_x \end{pmatrix}, \quad (\text{A2})$$

corresponding to couplers with  $180^\circ$  rotational symmetry, where  $\theta_x$  is the coupling parameter in the  $x$  direction. The discussion could also be generalized to arbitrary  $2 \times 2$  unitary coupling matrices of the form

$$S_\mu = e^{i\Phi_\mu^3} \begin{pmatrix} \sin \theta_\mu e^{-i(\Phi_\mu^1+\Phi_\mu^2)} & i \cos \theta_\mu e^{i(\Phi_\mu^1-\Phi_\mu^2)} \\ i \cos \theta_\mu e^{-i(\Phi_\mu^1-\Phi_\mu^2)} & \sin \theta_\mu e^{i(\Phi_\mu^1+\Phi_\mu^2)} \end{pmatrix},$$

where  $\{\Phi_\mu^1, \Phi_\mu^2, \Phi_\mu^3\}$  are additional Euler angles. Apart from some phase shifts in the wave amplitudes, these additional Euler angles may cause systematic shifts in  $k$  and  $\phi$ ; however, such shifts do not alter the topological properties of the network's bandstructure.

The coupling relation at the other node is given by

$$\begin{pmatrix} e^{ik-\gamma_2-i\phi}\psi_{\text{out}}^L \\ \psi_a \end{pmatrix} = S_y \begin{pmatrix} e^{\gamma_4+i\phi}\psi_{\text{in}}^L \\ \psi_b \end{pmatrix}. \quad (\text{A3})$$

We can use Eqs. (A1) and (A3) to obtain an analytic relation of the form

$$\begin{pmatrix} \psi_{\text{out}}^R \\ \psi_{\text{in}}^R \end{pmatrix} = M \begin{pmatrix} \psi_{\text{in}}^L \\ \psi_{\text{out}}^L \end{pmatrix}, \quad (\text{A4})$$

where  $M$  is the transfer matrix for one subunit. For a supercell of  $N$  subunits, we have

$$\begin{pmatrix} \psi_{\text{out}}^2 \\ \psi_{\text{in}}^2 \end{pmatrix} = \tilde{M} \begin{pmatrix} \psi_{\text{in}}^1 \\ \psi_{\text{out}}^1 \end{pmatrix}, \quad (\text{A5})$$

where  $\tilde{M} \equiv M^N$  is the total transfer matrix for the supercell. We can show that

$$\tilde{M} = \frac{\lambda_2^N - \lambda_1^N}{\lambda_2 - \lambda_1} M - \frac{\lambda_2^{N-1} - \lambda_1^{N-1}}{\lambda_2 - \lambda_1} \det(M),$$

where  $\lambda_{1,2}$  are eigenvalues of the transfer matrix  $M$ :

$$\lambda_{1,2} = \frac{\text{Tr}(M)}{2} \pm \sqrt{\left[\frac{\text{Tr}(M)}{2}\right]^2 - \det(M)}.$$

The outgoing and incoming wave amplitudes can then be related via the scattering matrix relation

$$\begin{pmatrix} \psi_{\text{out}}^1 \\ \psi_{\text{out}}^2 \end{pmatrix} = S_{\text{edge}} \begin{pmatrix} \psi_{\text{in}}^1 \\ \psi_{\text{in}}^2 \end{pmatrix}, \quad (\text{A6})$$

where

$$S_{\text{edge}} = \frac{1}{\tilde{M}_{22}} \begin{pmatrix} -\tilde{M}_{21} & 1 \\ \det(\tilde{M}) & \tilde{M}_{12} \end{pmatrix}. \quad (\text{A7})$$

## Appendix B: $\mathcal{PT}$ -symmetric 2D network

As mentioned in Section II, the non-Hermitian network that we have studied has gain and loss in certain links, but this gain/loss distribution is not  $\mathcal{PT}$  (parity/time-reversal) symmetric.<sup>32–36</sup> Alternatively, it is possible for us to impose a  $\mathcal{PT}$  symmetric gain/loss distribution on the network. Referring to Fig. 1(a), this can be accomplished by adding balanced gain and loss to links 1 and 3, and to links 2 and 4: i.e.,  $\gamma_1 = -\gamma_3$  and  $\gamma_4 = -\gamma_2$ .

In that case, the topological pump's  $S_{\text{edge}}$  matrix will

satisfy

$$\mathcal{PT}S_{\text{edge}}(-k, -\phi, -\gamma)\mathcal{PT} = S_{\text{edge}}^{-1}(k, \phi, \gamma), \quad (\text{B1})$$

where  $\mathcal{P}$  is the first Pauli matrix ( $\sigma_x$ ) and  $\mathcal{T}$  is the complex conjugation operator. Eq. (B1) is closely analogous to the symmetry relation obeyed by scattering matrices derived from  $\mathcal{PT}$  symmetric wave equations.<sup>35,36</sup>

For this  $\mathcal{PT}$  symmetric network, it can be shown that  $M \propto \exp(\gamma_1 + \gamma_4)$  and  $\tilde{M} \propto \exp[N(\gamma_1 + \gamma_4)]$ . The scattering matrix eigenvalues  $\{\sigma_n\}$  are thus independent of  $\gamma_1$  and  $\gamma_4$ . The system behaves like a Hermitian topological pump, regardless of the level of non-Hermiticity.

- 
- \* These two authors contributed equally to this work.  
 † yidong@ntu.edu.sg
- <sup>1</sup> M. Z. Hasan, and C. L. Kane, *Colloquium: topological insulators*, Rev. Mod. Phys. **82**, 3045 (2010).
  - <sup>2</sup> D. J. Thouless, M. Kohmoto, M. P. Nightingale, and M. den Nijs, Phys. Rev. Lett. **49**, 405 (1982).
  - <sup>3</sup> M. Stone, *Quantum Hall Effect* (World Scientific, 1992).
  - <sup>4</sup> L. Lu, J. D. Joannopoulos, and M. Soljačić, Nat. Photonics **8**, 821 (2014).
  - <sup>5</sup> Z. Yang, F. Gao, X. Shi, X. Lin, Z. Gao, Y. D. Chong, and B. Zhang, Phys. Rev. Lett. **114**, 114301 (2015).
  - <sup>6</sup> R. Fluery, A. B. Khanikaev, and A. Alù, *Floquet topological insulators for sound*, Nature Comm. **7**, 11744 (2016).
  - <sup>7</sup> D. Y. H. Ho, and J. B. Gong, Phys. Rev. Lett. **109**, 010601 (2012).
  - <sup>8</sup> B. A. Bernevig, and T. L. Hughes, *Topological insulators and topological superconductors*, Princeton University Press, 2013.
  - <sup>9</sup> F. Gao *et al.*, *Probing topological protection using a designer surface plasmon structure*, Nat. Comm. **7**, 11619 (2016).
  - <sup>10</sup> T. Kato, *Perturbation theory for linear operators*, volume 132 (Springer-Verlag, Berlin), 1966.
  - <sup>11</sup> W. D. Heiss, *The physics of exceptional points*, J. Phys. A: Math. Theor. **45**, 444016 (2012).
  - <sup>12</sup> Y. Hatsugai, *Chern Number and Edge States in the Integer Quantum Hall Effect*, Phys. Rev. Lett. **71**, 3697 (1993).
  - <sup>13</sup> M. S. Rudner and L. S. Levitov, Phys. Rev. Lett. **102**, 065703 (2009).
  - <sup>14</sup> K. Esaki, M. Sato, K. Hasebe, and M. Kohmoto, *Edge states and topological phases in non-Hermitian systems*, Phys. Rev. B **84**, 205128 (2011).
  - <sup>15</sup> C. E. Bardyn, M. A. Baranov, C. V. Kraus, E. Rico, A. mamolu, P. Zoller, and S. Diehl, New J. Phys. **15**, 085001 (2013).
  - <sup>16</sup> K. Ding, Z. Q. Zhang, and C. T. Chan, Phys. Rev. B **92**, 235310 (2015).
  - <sup>17</sup> T. E. Lee, *Anomalous Edge State in a Non-Hermitian Lattice*, Phys. Rev. Lett. **116**, 133903 (2016).
  - <sup>18</sup> D. Leykam, K. Y. Bliokh, C. Huang, Y. D. Chong, and F. Nori, *Edge Modes, Degeneracies, and Topological Numbers in Non-Hermitian Systems*, Phys. Rev. Lett. **118**, 040401 (2017).
  - <sup>19</sup> R. B. Laughlin, *Quantized Hall conductivity in two dimensions*, Phys. Rev. B **23**, 5632 (1981).
  - <sup>20</sup> P. W. Brouwer, *Scattering approach to parametric pumping*, Phys. Rev. B **58**, R10135 (1998).
  - <sup>21</sup> D. Meidan, T. Micklitz, and P. W. Brouwer, *Topological classification of adiabatic processes*, Phys. Rev. B **84**, 195410 (2011).
  - <sup>22</sup> I. C. Fulga, M. Maksymenko, *Scattering matrix invariants of Floquet topological insulators*, Phys. Rev. B **93**, 075405 (2016).
  - <sup>23</sup> L. W. Zhou, H. L. Wang, D. Y. H. Ho and J. B. Gong, Euro. Phys. J. B **87**, 1434 (2014).
  - <sup>24</sup> W. Hu, J. C. Pillay, K. Wu, M. Pasek, P. P. Shum, and Y. D. Chong, Phys. Rev. X **5**, 011012 (2015).
  - <sup>25</sup> T. Kitagawa, M. S. Rudner, E. Berg, and E. Demler, *Exploring topological phases with quantum walks*, Phys. Rev. A **82**, 033429 (2010).
  - <sup>26</sup> T. Kitagawa, E. Berg, M. Rudner, and E. Demler, *Topological characterization of periodically driven quantum systems*, Phys. Rev. B **82**, 235114 (2010).
  - <sup>27</sup> D. Y. H. Ho and J. B. Gong, Phys. Rev. B **90**, 195419 (2014).
  - <sup>28</sup> H. L. Wang, L. W. Zhou, and J. B. Gong, Phys. Rev. B **91**, 085420 (2015).
  - <sup>29</sup> N. H. Lindner, G. Refael and V. Galitski, *Floquet topological insulator in semiconductor quantum wells*, Nat. Phys. **7**, 490 (2011).
  - <sup>30</sup> M. Pasek, and Y. D. Chong, *Network models of photonic Floquet topological insulators*, Phys. Rev. B **89**, 075113 (2014).
  - <sup>31</sup> H. L. Wang, L. W. Zhou, and Y. D. Chong, *Floquet Weyl phases in a three-dimensional network model*, Phys. Rev. B **93**, 144114 (2016).
  - <sup>32</sup> C. M. Bender and S. Boettcher, Phys. Rev. Lett. **80**, 5243 (1998).
  - <sup>33</sup> C. M. Bender, M. V. Berry, and A. Mandilara, J. Phys. A **35**, L467 (2002).
  - <sup>34</sup> K. G. Makris, R. El-Ganainy, D. N. Christodoulides, and Z. H. Musslimani, Phys. Rev. Lett. **100**, 103904 (2008).
  - <sup>35</sup> Y. D. Chong, L. Ge, and A. D. Stone, Phys. Rev. Lett. **106**, 093902 (2011).
  - <sup>36</sup> Y. D. Chong and M. C. Rechtsman, *Tachyonic dispersion in coherent networks*, J. Opt. **18**, 014001 (2015).
  - <sup>37</sup> R. Uzdin, A. Mailybaev, and N. Moiseyev, *On the observability and asymmetry of adiabatic state flips generated by exceptional points*, J. Phys. A: Math. Theor. **44**, 435302 (2011).